Journal of Alloys and Compounds 722 (2017) 920-927
Doi: 10.1016/j.jallcom.2017.06.160

Ga-doped ZnO self-assembled nanostructures obtained by microwave-assisted hydrothermal synthesis: effect on morphology and optical properties

M.S. Bernardo[1*], P.G. Villanueva[1], T. Jardiel[2], D.G. Calatayud[2], M. Peiteado[1, 2] and A.C. Caballero[2].

[1]POEMMA-CEMDATIC, ETSI Telecomunicación (UPM), 28040 Madrid, Spain

[2]Department of Electroceramics, Instituto de Cerámica y Vidrio (CSIC), 28049 Madrid, Spain

*Corresponding author: tel. + 34917355840; Fax: + 34917355840; e-mail address: mara.bernardo@upm.es , mbernardo@icv.csic.es

Abstract

Highly homogeneous gallium doped ZnO assembled nanostructures comprised by thin hexagonal platelets showing a striking preferred orientation along the ab plane have been obtained by an ultra-fast and eco-friendly microwave assisted hydrothermal synthesis method. Although the incorporation of gallium into the ZnO lattice is found to be relatively low, namely ≤ 1 mol.%, the gallium nitrate addition plays a key role in the size and morphology of the obtained ZnO nanostructures. The observed morphology is attributed to the selective adsorption of the gallium species on the basal planes of ZnO, which inhibits the growth along the ± [0001] direction. Additionally, the optical band-gap and the fluorescence emission are modified upon gallium addition. The observed changes in the optical properties are ascribed to both the decreased crystal size and to the gallium incorporation into the ZnO structure, which lead to the modification in the energy levels.

Keywords:

Zinc oxide; gallium-doping; microwave-assisted hydrothermal synthesis; capping agent; sustainable processing.

Journal of Alloys and Compounds 722 (2017) 920-927
Doi: 10.1016/j.jallcom.2017.06.160

1. Introduction.

ZnO is a semiconductor material which presents a set of unique physicochemical properties, such as piezoelectricity, a direct wide band-gap of 3.37 eV at 298 K and large excitation binding energy of 60 meV [1-3]. These properties make ZnO a versatile functional material with a wide range of applications such as chemical sensors and biosensing, piezoelectric transducers and actuators, catalysts, transparent semiconductors and different optoelectronic devices [1-9]. Accordingly, a large number of studies put their focus on tuning the physicochemical properties of ZnO to fit the requirements of a particular application, this being critical to enhance the performance of novel devices. For example, in the particular case of optoelectronic applications it is well known that the properties are highly dependent on its impurity level since the chemistry of defects plays a key role [3,10,11]. Therefore, initially a very useful way to tune the electronic and optical properties in ZnO is through doping. Particularly, elements of group III (Al, In, Ga), which have comparatively higher energy states and strongly hybridize with conduction band states of oxide semiconductors, can generate free electrons when doping ZnO and, consequently, can fill up the conduction band levels [11-14]. Among these dopants, Ga^{3+} is especially attractive due to its relatively low cost, its non-toxicity and the high similarity among the ionic radii of Ga^{3+} (0.61 Å) and Zn^{2+} (0.74 Å) [15]. Thus, gallium-doped ZnO (usually denoted as GZO) is a specially promising material suitable for many innovative applications due to its high carrier concentration and electrical conductivity [6,7,10,16-21]. But in addition to doping, the electronic and optical properties of ZnO depend closely on the microstructural characteristics of the material, this including the crystal size, the crystal orientation and aspect ratio, the crystalline density, as well as the surface area and morphology (how the crystals are stacked) [22]. In this sense, tailoring the morphology during the fabrication process represents another fruitful strategy to modulate the ZnO properties [1-4,23-27]. This obviously obliges to a precise control over the crystal growth habit and several factors should then be considered when devising a specific functional (micro)nanostructure. Namely, both the specific experimental conditions and the intrinsic crystal structure of ZnO have a decisive influence on the crystallization engineering. On one hand würtzite ZnO crystallizes in a hexagonal structure (space group *C6mc*) that can be described as a number of alternating planes stacked along the c-axis and composed of tetrahedrally coordinated O^{2-} and Zn^{2+} ions. The tetrahedral

coordination results in a non-centrosymmetric structure with polar surfaces (the oppositely charged ions produce positively charged Zn-(0001) and negatively charged O-$(000\bar{1})$ surfaces), which originates a normal dipole moment and a spontaneous polarization along the c-axis. As a straight consequence, a divergence in energy is created with the ±(0001) polar surfaces having a higher surface energy than the remainder non-polar prismatic facets. Certainly, these different surface characteristics of ZnO will induce anisotropic growth. Under thermodynamic equilibrium conditions, the growth along the c-axis is favour respect to the growth in the prismatic directions to reduce the surface energy and, hence, the facet with higher surface energy will result smaller in area than the lower energy facets [1]. Consequently, large arrays of ZnO nanostructures can be grown relatively easy along the c-axis [28-31]. However, as mentioned, the experimental conditions of the fabrication procedure can also play a decisive role on the crystal development. Clearly, growing ZnO extended nanostructures oriented along crystallographic directions other than the expected c-axis oriented rods is very appealing and efforts are being conducted in this direction. Nowadays a high degree of crystallographic control can be achieved using film deposition techniques like electron-beam evaporation, molecular beam epitaxy, pulsed laser deposition and the like [32-35]. All these techniques however involve high energy operations in terms of temperature, pressure and sophisticated equipment. Obviously, superlative benefits like simplicity, cost efficiency or environmental benevolence can be expected if sustainable processes would be used instead and, in this sense, several bottom-up solution-based techniques are currently being considered to prepare different ZnO based nanostructures. Among the different available strategies, the hydrothermal processing approach results particularly interesting because it is a low-energy consuming solution-based process which can allow the sustainable fabrication of ZnO structures with tailored size, morphology and orientation [31,36-40]. More recent works describe the preparation of ZnO structures using an alternative hydrothermal strategy based on the adjustment of the exterior reaction environment by the simultaneous application of microwave radiation, i.e. a so called microwave-assisted hydrothermal (MAH) process [41-46]. Visibly the concurrent use of microwave heating can render additional benefits related to energy and time saving, but it may be useful as well to avoid “conventional” hydrothermal inconveniences, such as sharp thermal gradients throughout the bulk solution, non-uniform reaction conditions and/or slow reaction

(crystallization) kinetics [47-49]. Last but not least, in addition to the specific conditions of the MAH process (pH, temperature and time, pressure, MW powder) further changes in morphology can be addressed from the action of external species, such as capping agents, that can act as promoters or inhibitors of the nucleation and growth processes [22,37,50]. Generally speaking, these molecules can tailor the surface energy of the synthesized nuclei by capping the growth in one or more faces, so making the crystal develop only in certain directions and, hence, altering/controlling its morphology [51-53]. Typically, capping agents are organic molecules (such as surfactants or polymers), but it has been recently described that some inorganic species may as well provide a new effective way to control the shape and size of the hydrothermally grown ZnO particles [37]. These species might have been added to the composition with the purpose of doping the nanocrystal lattice. Thus, in such a case the dopants would have a double effect on the material: microstructural and functional [37,54]. Therefore, within this frame, the present contribution describes the preparation of gallium doped ZnO oriented nanostructures by using a microwave-assisted hydrothermal method. Added as gallium nitrate to the precursor solution in the autoclave reactor, the effect of this dopant on both the morphology and crystallographic orientation of the as-obtained ZnO nanostructures (capping agent effect), as well as on their resulting optical properties (net incorporation to the wurtzite lattice) is described.

2. Experimental procedures

Ga-modified ZnO powders with nominal composition $Zn_{1-x}Ga_xO$, with x ¼ 0, 0.005, 0.01 and 0.03 -hereby denoted as ZnO, GZO-0.5%, GZO-1% and GZO-3%- were synthesized via a microwave- assisted hydrothermal (MAH) method. First, the corresponding stoichiometric amounts of zinc acetate, $Zn(CH_3CO_2)_2{\cdot}2H_2O$, and gallium nitrate, $Ga(NO_3)_3{\cdot}xH_2O$, were dissolved in 40 ml of H_2O. Then, 10 ml of KOH 1 M were added into the intermetallic solution for the co-precipitation of the corresponding hydroxides. The nominal $Zn_{1-x}Ga_xO$ concentration in the final suspension was 0.1 M. Then, 50 ml of this mixture were poured into a Teflon vessel of 220 ml that was placed into a commercial Milestone ETHOS 1 microwave apparatus, operating at 2450 MHz and equipped with temperature and pressure sensors that enable a full control of the most important reaction parameters. Reactions were carried out at 180 ºC during 15 min, with heating and cooling slopes of 15 min, the microwave power limited to 250 W

and autogenous pressure, which was monitored during the experiments. After reaction, the solid product was washed several times with distilled H_2O and, subsequently, with ethanol. Finally, the powders were dried at 60 ºC during 24 h.

The chemical composition of the obtained powders was analysed by inductively coupled plasma optical emission spectrometry (ICP-OES) on a Thermo Jarrel Ash Atomscan 25 spectrometer. The powders were also characterized through X-ray diffraction (XRD) on a Bruker D8 Advance diffractometer using Cu Ka1 radiation (λ = 1.5406 Å). XRD samples were prepared by placing a few drops of a concentrated ethanol dispersion of particles onto a single crystal silicon plate. Step-scanned X-ray diffraction patterns were collected between 15 and 90º in steps of 0.02º and with a counting time of 1.5 s per step. The morphology of the particles was analysed by using a cold field emission scanning electron microscope (FESEM, model S-4700 Hitachi). UV-vis diffuse reflectance spectroscopy (DRS UV-vis) was carried out on a UV-Vis-NIR Varian Cary 5000 spectrometer equipped with an integrating sphere. Fluorescence spectroscopy measurements were performed on a Varian Cary Eclipse Fluorescence spectrophotometer. The measurements were conducted in solid state with an excitation wavelength set at 264 nm.

3. Results

3.1 Chemical composition

The actual chemical composition of the synthesized powders was analysed by ICP-OES. For each particular sample, Table 1 compares the expected gallium concentration according to the formulated nominal composition ($Zn_{1-x}Ga_xO$) with the molar gallium concentration as measured by ICP. It is observed that for samples with low gallium content in the nominal composition, i.e. $x \leq 0.01$, the obtained results are in a very good agreement with those expected according to the formulated composition. But, in contrast, for samples formulated with $x > 0.01$ the actual gallium concentration remains almost constant. The chemical composition was also analysed by X-ray fluorescence and results (not shown here) were in good agreement with those obtained by ICP-OES.

Accordingly, it seems that only a partial amount of the gallium added to these compositions remains in the synthesized material, while the excess of gallium added to

the samples with x > 0.01 is being rinsed from the powder during the washing processes. Moreover, these results also indicate that under the applied MAH synthesis conditions the solid solution limit for the $Zn_{1-x}Ga_xO$ compound, if existing, should be ≤ 1 mol %.

Sample	x	Expected [Ga] (Formulated composition) (mol.%)	Actual [Ga] (ICP-OES) (mol.%)
ZnO	0	0.00	0.00
GZO-0.5%	0.005	0.50	0.47 ± 0.01
GZO-1%	0.01	1.00	0.89 ± 0.01
GZO-3%	0.03	3.00	1.17 ± 0.01

Table 1. Expected gallium concentration according to the formulated nominal composition and real concentration as measured by ICP-OES analyses.

3.2 Crystalline structure and morphology

The powder X-ray diffractograms of samples with different gallium concentrations are depicted in Fig.1. All the observed peaks can be indexed according to the würtzite-type structure of ZnO (ICDD No. 00-036-1451); no other diffraction maximum that may indicate the presence of different crystalline phase(s) was ever observed. On the other hand, the comparison of the patterns belonging to samples with and without gallium does not show any significant shift in the position of the ZnO peaks. As a matter of fact, the small amount of gallium present in these samples (1 mol % in the best scenario, Table 1) can impede its proper identification by XRD. In agreement with the chemical analyses, this may again indicate that the incorporation of gallium into the ZnO lattice as a stable solid solution, if produced, is very limited. Lastly, some differences were observed in the intensity of the ZnO peaks that may be related to differences in the aspect ratio of the ZnO crystals and/ or to a different orientation of the particles. The crystallite size along the c-axis of samples with different gallium content was estimated by using the Scherrer equation on the (002) X-ray diffraction peak. Results yielded to a crystallite size of about 310, 180, 110 and 100 nm for the ZnO, GZO-0.5%, GZO-1%

and GZO-3%, respectively, pointing out to a decrease in the crystal size as the gallium concentration increases.

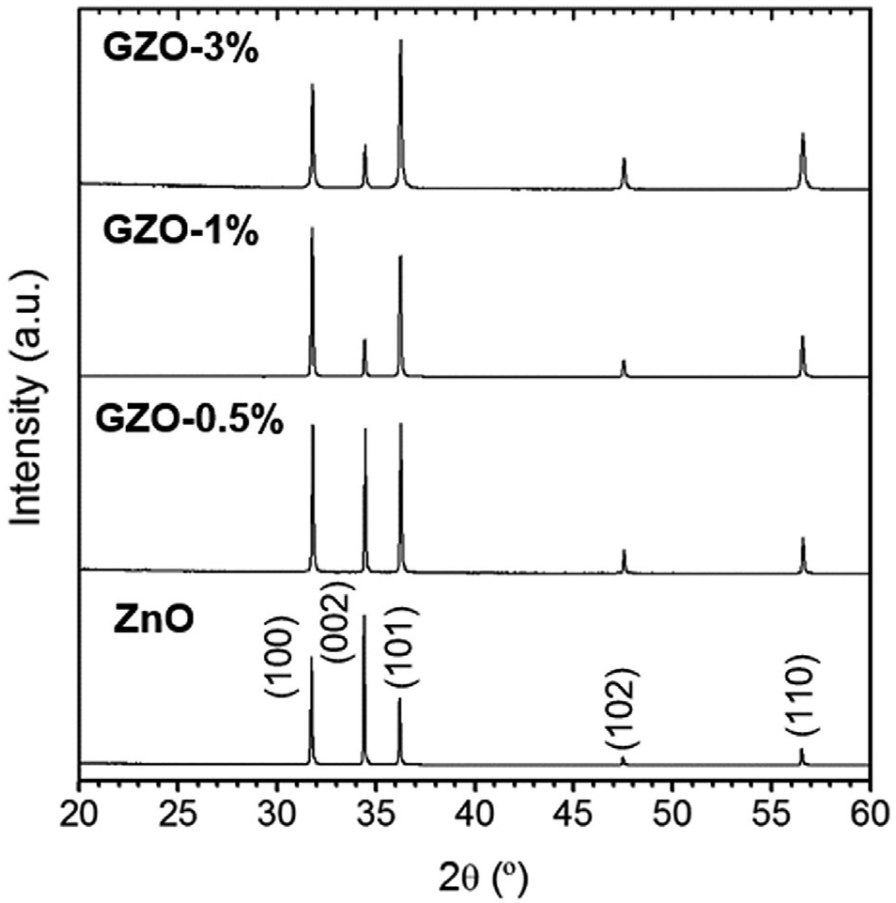

Fig. 1. Normalized powder XRD of $Zn_{1-x}Ga_xO$ samples with x = 0, 0.005, 0.01 and 0.03.

The morphology of the different samples was studied by field emission scanning electron microscopy (FESEM). For the undoped ZnO composition (Fig. 2 a and b) a homogeneous population of micron-sized rods (slightly above 1 mm in length) is obtained, with each rod showing characteristic hexagonal dumbbell-like bipod shape. As mentioned above, due to the polar structure of ZnO, the growth along the c-axis leading to the development of a rod-like morphology is favoured under thermodynamic equilibrium and, actually, these conditions can be easily achieved during the hydrothermal synthesis. That is to say, the rod-like morphology is quite usual for ZnO particles obtained by hydrothermal processes. However, it is worth to mention that the experimental conditions here applied further enable the preparation of a product powder with a high degree of homogeneity in size and shape. On the other hand, the

micrographs of the sample formulated with 0.5 mol % of gallium (GZO-0.5%) show that particles constituting the ceramic powder are considerably smaller than that of the undoped composition (see Fig. 2c). Regarding the morphology, some clear differences can be enumerated too. First, although the particles still draw the standard rod-like shape, a relatively lower homogeneity in morphology is now observed: the dumbbell-like morphology is visibly less frequent and actually some of the bipods have lost their symmetrical structure leading to some sort of asymmetrical units. But moreover, higher magnification images also indicate that the obtained particles could rather be formed by the organized assembly of smaller units. Namely, Fig. 2 d shows that such smaller units are actually hexagonal nanoplatelets with an average diameter of 200-300 nm and a thickness of just few tens of nanometers. This particular aggregative configuration is much clearer observed by FESEM when further increasing the amount of gallium in the starting formulation. As seen in Fig. 2 e and f corresponding to the sample with a nominal 1 mol % of gallium (GZO-1%), the higher amount of dopant first produces an increased size of the particle aggregates, which morphology consist in highly homogeneous symmetrical rods that again show a predominant dumbbell-like bipod morphology. These rods show a length of around 2 mm and, as mentioned, it is now more manifest that they are formed by pilled stacks of hexagonal platelets. These platelets are larger too, now reaching an average diameter of ~1 mm which doubles the diameter of the platelets in the GZO-0.5% powder, but interestingly, they keep the same thickness (just a few tens of nanometers). Finally, samples formulated with a higher concentration of gallium, 3 mol %, were also analysed by FESEM. The morphology and the size of the particles composing this GZO-3% powder (not shown here) were indistinguishable from that of the GZO-1% sample: 2 mm length rod-like aggregates composed by individual platelets of 1 mm in diameter and just 20-30 nm in thickness. The microstructural similitudes between these two powders can be related to the fact that both samples have the same content of gallium, ca. 1 mol %, as indicated in Table 1.

So, at this point the FESEM microstructural characterization evidences that the gallium addition primarily has a strong effect on the morphology of the obtained particles and it greatly modifies the aspect ratio of the hexagonal ZnO crystals that constitute the observed nanostructures, as illustrated in Fig. 3. While in the absence of gallium a distinctive rod-like structure is produced with a much larger length (or thickness) than

width (diameter), the presence of a small amount of gallium provokes a drastic reversion in the aspect ratio and the crystal shape evolves to a platelet-like structure which is now larger in diameter than in thickness.

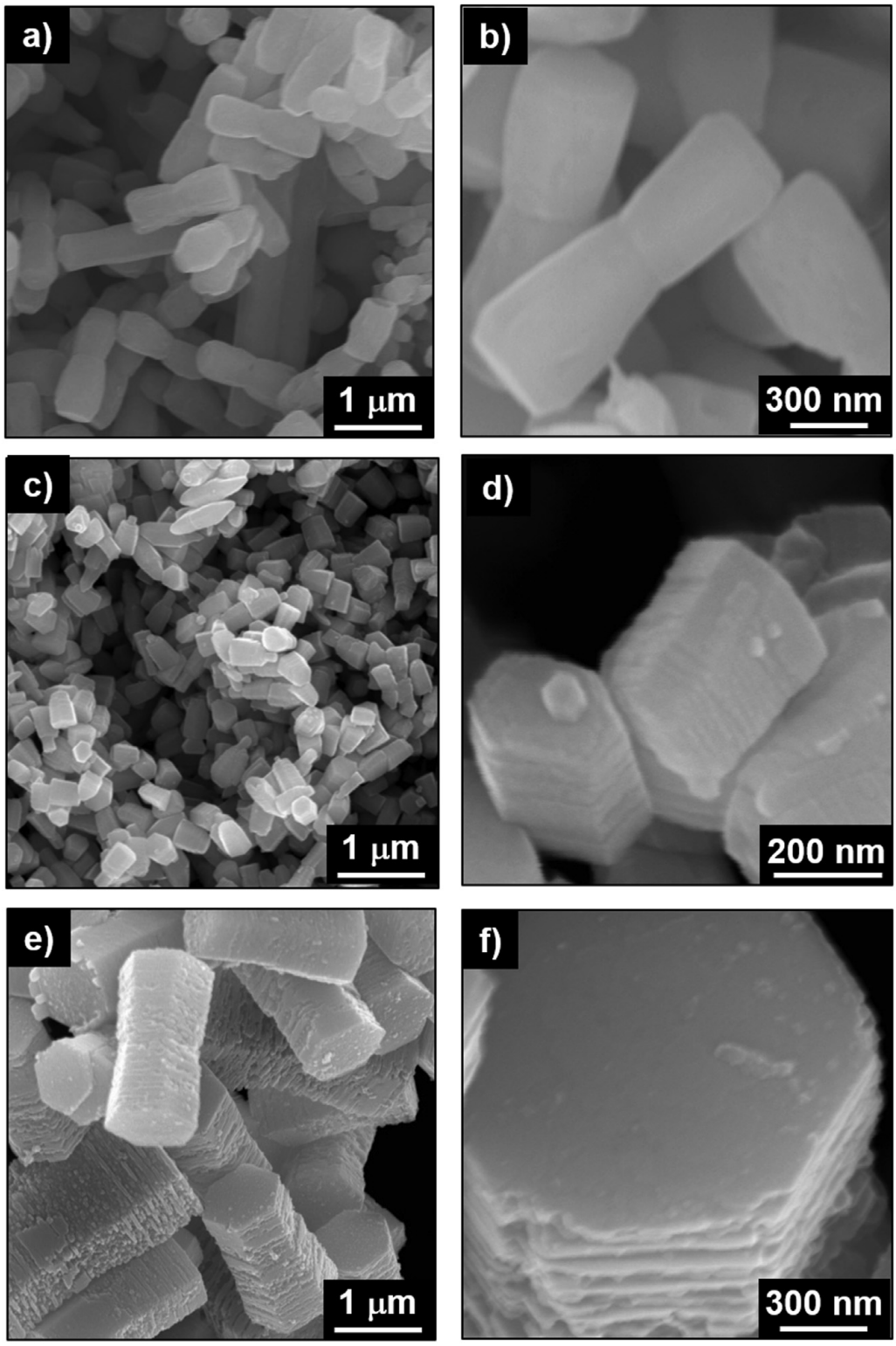

Fig. 2. FESEM images of ZnO (a and b), GZO-0.5% (c and d) and GZO-1% (e and f) powders.

Moreover, further gallium additions (≥ 1 mol. %) lead to platelets with even bigger diameters while the thickness remains almost constant. It is worth to note that, although the reaction conditions under the MAH synthesis (especially, MW power) can influence the size and the aspect ratio of the ZnO particles [44], the obtained structures typically show a rod-like morphology with larger height than width. In contrast, the changes in the aspect ratio of the hexagonal crystals here observed upon the addition of gallium are much more noteworthy.

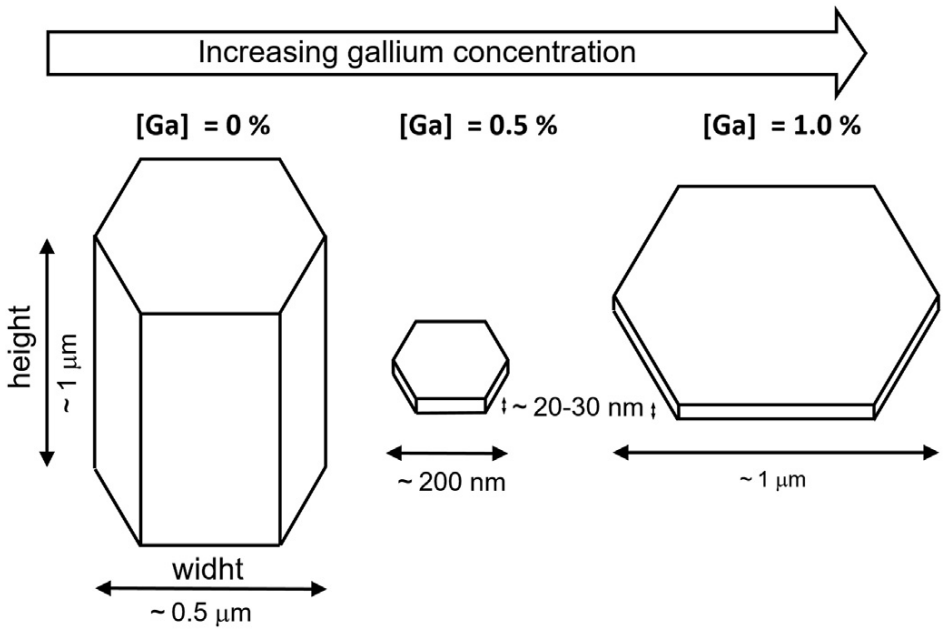

Fig. 3. Schematic illustration of the variation of the aspect ratio of the hexagonal ZnO crystal units that comprise the observed nanostructures as a function of the gallium concentration.

3.3 Optical and photoluminescence properties.

First, UV-vis spectroscopy was carried out to investigate the light absorption behavior of materials and calculate the band-gap values. Fig. 4 shows the optical absorption spectra of ZnO and GZO compositions. As it can be observed from the figure, the absorption of the GZO-0.5% sample is blue shifted with respect to the pure ZnO, higher band-gap, but when the percentage of Ga is increased over 1%, the absorption peak is red shifted compared with the pure ZnO, i.e. a decrease in the band-gap value. The inset of Fig. 4 shows the Tauc-plot from which the band-gap values were calculated (Table 2). While the pure ZnO shows a value of 3.23 eV, the GZO-0.5% composition presents a higher value (3.28 eV). When the percentage of gallium reaches the 1%, the band-gap

values stabilize and are close to 3.19 eV, due to the fact that all these samples have a similar concentration of gallium as indicated by the chemical analysis. These results suggest that the chromatic shift is mainly due to the incorporation of gallium into the ZnO lattice, which produces a decrease in the band-gap values. The band-gap is also affected by the size and morphology of the particles [55], which can explain the higher band-gap values of GZO-0.5% with respect to the pure ZnO. The GZO-0.5% composition presents a low concentration of gallium and, although the Ga^{3+}-doping decreases the band-gap, this effect is not strong enough to compensate the increasing of the band-gap produced by the reduction of the size of the particles and their change of morphology.

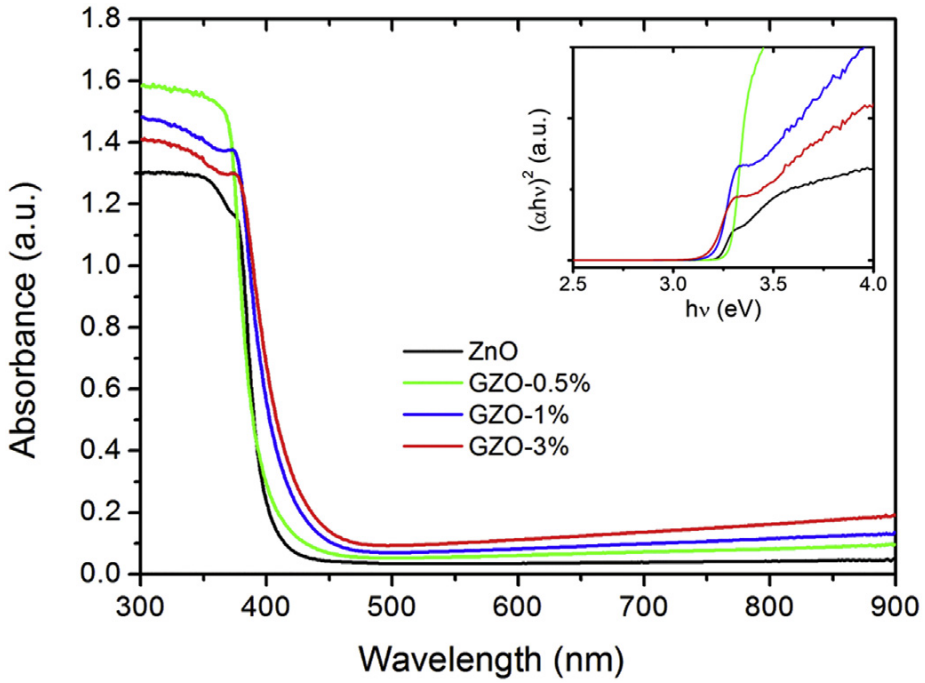

Fig. 4. UV-Vis spectra of samples with different gallium nitrate additions. The inset shows the Tauc-plot from which the band gap values were calculated.

Sample	**Eg (eV)**
ZnO	3.23
ZG005	3.28
ZG01	3.20
ZG03	3.18

Table 2. Band-gap values calculated from the UV-Vis spectra.

To investigate the fluorescence emission behavior of the GZO samples fluorescence spectroscopy was performed. In Fig. 5 the emission spectra (λexc = 264 nm) for all the compositions show 9 emission peaks at 361 nm, 394 nm, 416 nm, 433 nm, 441 nm, 446 nm, 460 nm, 484 nm and 493 nm. As shown in Fig. 5, the increasing of gallium content into ZnO results in a modification of the relative intensity of the peaks at 394 nm, 416 nm, 433 nm and 493 nm, with respect to the peak at 484 nm. The intermediate levels within the band gap region determine the emission features and are generated by the produced defects. Physics and chemistry of defect formation and variation of defect concentration in ZnO are very complex [16].

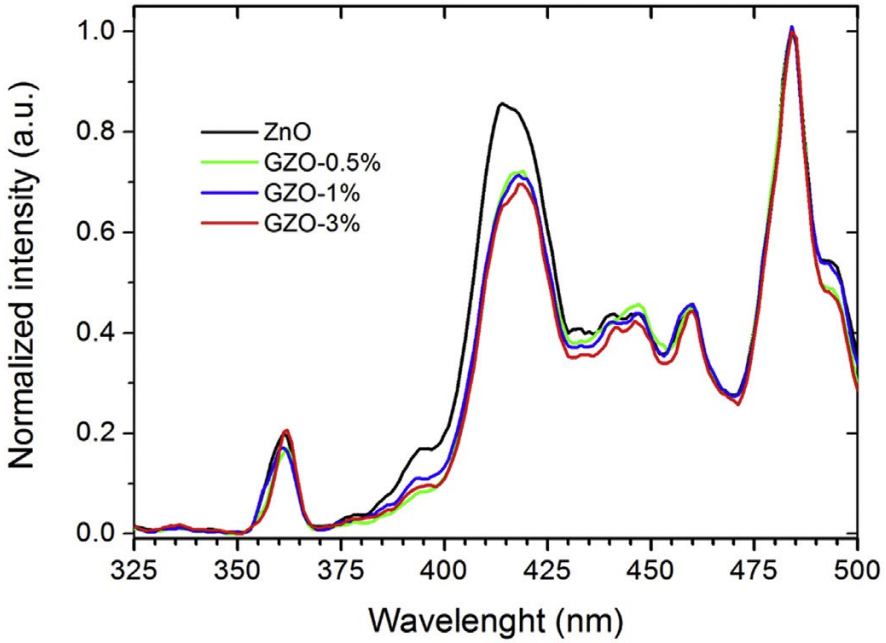

Fig. 5. Fluorescence emission spectra of samples with different gallium concentration. (λexc = 264 nm).

As reported by Saha et al. [16], most of the vacant tetrahedral and octahedral lattice sites of the relatively open crystal structure of ZnO favour both intrinsic and extrinsic interstitial defects. Different types of defects in ZnO nanocrystals create some localized donor states like shallow trap states near the conduction band and acceptor states or deep trap states near the valence band. In this, sense doping with Ga^{3+} influences the intrinsic defect states of ZnO significantly. Experimentally and theoretically it is found that Ga^{3+} induces V_{Zn} in ZnO crystals due to self-charge compensation [56]. Moreover, Ga^{3+} can also occupy both substitutional (Ga_{Zn}) and interstitial sites (Ga_i) of the ZnO lattice [57]. Furthermore, for larger Ga^{3+} concentrations, vacancy complexes such as

Ga_{Zn}–V_{Zn} and Ga_{Zn}–O_i can be formed due to strong Coulomb interaction; these complexes would affect mainly deep acceptor states. Thus, a large variety of defect levels control the emission bands in the visible region due to multiple transitions depending on available states of each defect level. In our case, the modification of the relative intensity of the fluorescence emission peaks is similar in all the doped samples independently of the gallium percentage. It is known that the optical properties of GZO possess nontrivial dependence on the doping concentration, especially when doped as close to the solid-solubility limit as possible [20]. Nevertheless, the observed change in the energy levels upon gallium addition indicates that a certain amount of gallium is being incorporated into the ZnO structure.

4. Discussion

To understand the morphological development produced with increasing gallium additions, it should be taken into account that all the species presented in the reaction media, such as the employed base or the counter-ions of the zinc and the dopant(s) precursors, might affect the crystalline morphology during the synthesis [58-62]. In our case, the simplicity of the described MAH procedures may enable an easier understanding of the role of each specie on the morphology of the obtained ZnO-based nanostructures. Namely, the only additives employed are those arising from the KOH base -which was kept identical for all the samples with different gallium content- and the corresponding acetates and nitrates from the Zn^{2+} and Ga^{3+} precursors, respectively -which ratio varies as a function of the formulated composition. And, the fact is that the effect of both acetates and nitrates anions has been has been widely studied for undoped ZnO. On one hand, in the presence of acetates the formation of layered basic zinc acetate (LBZA) usually determine the typical layered crystallization morphologies, e.g. flakes, needles or thin elongated plates [63]. On the other hand, the excess of nitrates usually enhances the formation of well crystallized ZnO rods of large sizes [64]. In our experiments it is observed that the formation of platelets is favour as the ratio among acetates and nitrates coming from the Zn^{2+} and Ga^{3+} precursors increases. This suggests that the excess of nitrates may influence the axial growth of the nanoplatelets, while the growth inhibition along the c-axis shall be related to the Ga^{3+} ions.

As mentioned in the introduction, certain species, so-called capping agents, can tailor the morphology of hydrothermally synthesized particles by selectively absorbing on certain surfaces and, hence, capping the growth in the corresponding crystallographic directions [51,52]. The microstructural evidences described in the previous section indicate that the gallium species must be mainly located at the external surfaces of the ZnO crystals, where they play a decisive capping role that controls their growth and morphological development. In fact, it is well known that when doping semiconductor nanocrystals with well-defined facets, the initial adsorption of impurities on certain nanocrystal faces is critical for a successful incorporation of the dopant into the lattice [65]. The changes in the optical response of the MAH synthesized samples upon gallium addition evidence that a certain amount of dopant is actually being incorporated into the ZnO lattice, although in agreement with the chemical analyses and the XRD (indicating that the cell parameters barely vary with increasing gallium additions) the incorporation of gallium is very limited, i.e. $\leq$ 1 mol.%, and a stable solid solution is far to be produced. Thus, due to the low solid solution limit the dopant tends to segregate and, hence, preferentially locates close to the nanocrystals surface. In fact, this kind of behaviour is very common for different semiconductor materials doped with donors in which, once the system reaches the solid solution limit which is indeed very low, the dopant tends to segregate and, eventually, inhibits the crystal growth [66-68].

Accordingly, a plausible mechanism explaining the morphological development for the MAH synthesized GZO nanostructures can be suggested as follows and it is depicted in Fig. 6. In the undoped ZnO samples the formation of rod-like structures is attributed to the intrinsic polar structure of wurtzite ZnO, as explained above. However, when gallium nitrate is added to the composition, it selectively adsorbs onto the ± (0001) polar surfaces of the ZnO nanocrystal nuclei. This obviously impedes the adsorption of new (ZnO) growing units on those faces, i.e, blocks the diffusion processes along that direction and, consequently, the crystalline growth along the c-axis is inhibited. Then, further crystal enlargement could only occur by means of growing along the ab plane (along the prismatic directions of ZnO), this leading to the formation of platelets instead of rods. It is important to mention that the differences in the size and aspect ratio when the gallium concentration increases from 0.5 to 1 mol % can be related with the competition among the formation of new crystallization nuclei and the growth along the ab plane once the fast crystallization along the c-axis is blocked. It seems that in the

presence of a low gallium nitrate concentration (i.e. 0.5 mol %) the nucleation prevails, while in the presence of higher gallium nitrate additions the crystal growth becomes more predominant -which is also influenced by the excess of nitrates presented in the reaction media-, this resulting in larger platelets with higher aspect ratio. But the fact is that the formation of the platelets would eventually lead to a thermodynamically unfavourable situation: in the platelet morphology the facets with the higher surface energy (the polar ones) are predominant, that is to say, they are more exposed to the medium. So, initially the resulting crystals will show an unstable high surface energy. And obviously, the higher the aspect ratio of the platelet, the higher will be the surface energy and the instability of the obtained powder. To overcome this scenario the hexagonal platelets tend to assemble parallel to each other due to the long range electrostatic interactions among the polar (0001) planes. The result is the formation of the observed nanostructured aggregates showing a rod-like morphology but composed of parallel stacked platelets with a thickness of just a few tens of nanometers. It is known that during the MAH processes the microwave electrical field can assist in the oriented attachment of crystals with high dipole moments [69]. Thus, in our case it is likely that the microwave radiation also aids in the self-assembling of the platelets in parallel to their major dimension (basal plane).

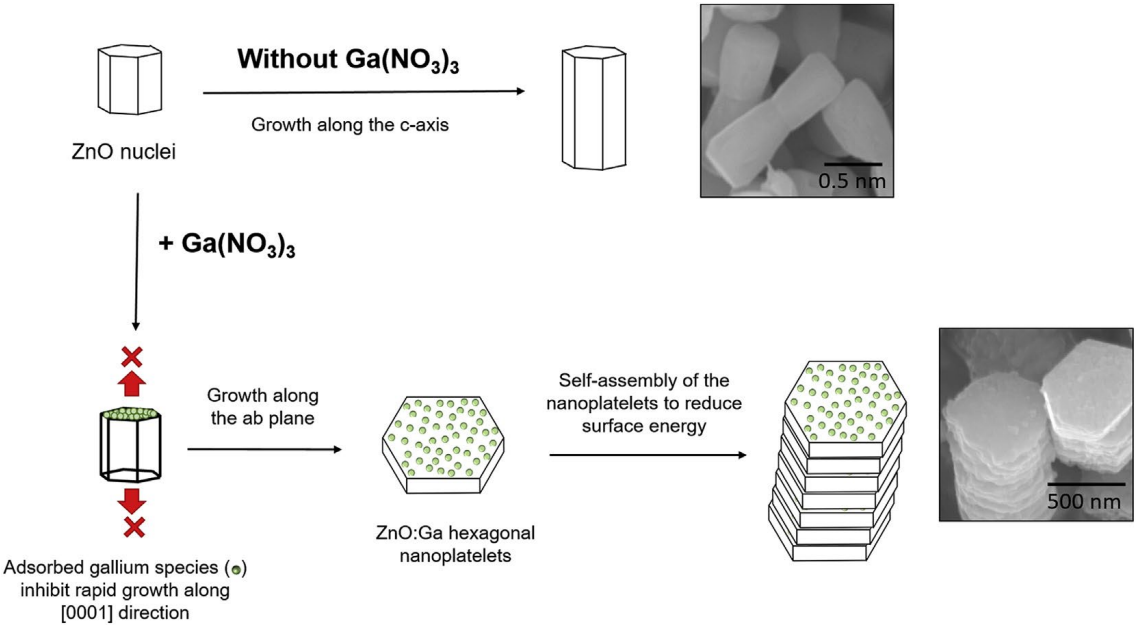

Fig. 6. Proposed mechanism for the crystallization and assembly of the ZnO-based particles with and without gallium addition.

5. Conclusions

Undoped and gallium-doped ZnO powders have been synthesized by a sustainable microwave-assisted hydrothermal method. The chemical analyses and the X-ray diffractograms indicate that the $Zn_{1-x}Ga_xO$ solid solution limit under these synthesis conditions is relatively low, i.e. ≤ 1 mol %. Even though, the addition of such small amount of gallium plays a key role in the crystal development by capping the growth along the c-axis. This leads to the formation of complex morphologies consisting in thin hexagonal platelets with highly exposed polar surfaces that eventually self-assemble parallel to each other to again produce a rod-like superstructure. Moreover, the optical properties can also be tuned with the addition of gallium, something which is ascribed to the observed changes in morphology as well as to a partial incorporation of gallium into the ZnO lattice. First, a decrease in the optical bandgap respect to the undoped material is achieved for gallium concentrations of 0.5 mol% whereas higher gallium concentrations produce a decrease of the band-gap values. On the other hand, the fluorescence emission is also modified upon gallium doping leading to a change in the relative intensity, which endures for higher amounts of dopant.

Acknowledgements

This work has been conducted within the MAT2013-40722-R, MAT2014-59210-JIN and MAT2016-80182-R projects. This work was also conducted in the frame of “Grupo de Propiedades Opticas, Electricas y Magneticas y sus Aplicaciones”, (UPM), Unidad Asociada al Instituto de Ceramica y Vidrio (CSIC).

References:

1. Wang, Z.L., Zinc oxide nanostructures: Growth, properties and applications. Journal of Physics Condensed Matter, 2004. 16(25): p. R829-R858.
2. Özgür, Ü., et al., A comprehensive review of ZnO materials and devices. Journal of Applied Physics, 2005. 98(4): p. 1-103.
3. Schmidt-Mende, L. and J.L. MacManus-Driscoll, ZnO - nanostructures, defects, and devices. Materials Today, 2007. 10(5): p. 40-48.
4. Wang, Z.L., Nanostructures of zinc oxide. Materials Today, 2004. 7(6): p. 26-33.

5. Jiménez Reinosa, J., et al., Enhancement of UV absorption behavior in ZnO–TiO_2 composites. Boletín de la Sociedad Española de Cerámica y Vidrio, 2016. 55(2): p. 55-62.
6. Thirunavukkarasu, K. and R. Jothiramalingam, Synthesis and structural characterization of Ga-ZnO nanodisk/nanorods formation by polymer assisted hydrothermal process. Powder Technology, 2013. 239: p. 308-313.
7. R. Jothi Ramalingam, T.R., Hamad A. Al-Lohedan, Preparation and surface characterization of nanodisk/nanoflower-structured gallium-doped zinc oxide as a catalyst for sensor applications. Chinese Journal of Catalysis, 2016. 37(8): p. 1235-1241.
8. Z.G. Zang, et al., Femtosecond laser direct writing of microholes on roughened ZnO for output power enhancement of InGaN light-emitting diodes, Opt. Lett. 41 (2016) 3463-3466.
9. Z. Zang, X. Tang, Enhanced fluorescence imaging performance of hydrophobic colloidal ZnO nanoparticles by a facile method, J. Alloys Compd. 619 (2015) 98-101.
10. Wang, R., A.W. Sleight, and D. Cleary, High Conductivity in Gallium-Doped Zinc Oxide Powders. Chemistry of Materials, 1996. 8(2): p. 433-439.
11. Sans, J.A., et al., Chemical effects on the optical band-gap of heavily doped ZnO: MIII (M=Al,Ga,In): An investigation by means of photoelectron spectroscopy, optical measurements under pressure, and band structure calculations. Physical Review B - Condensed Matter and Materials Physics, 2009. 79(19).
12. McCluskey, M.D. and S.J. Jokela, Defects in ZnO. Journal of Applied Physics, 2009. 106(7).
13. Lim, J.H., et al., Synergistic effect of Indium and Gallium co-doping on growth behavior and physical properties of hydrothermally grown ZnO nanorods. Scientific Reports, 2017. 7.
14. Sankar ganesh, R., et al., Influence of Al doping on the structural, morphological, optical, and gas sensing properties of ZnO nanorods. Journal of Alloys and Compounds, 2017. 698: p. 555-564.
15. Shannon, R.D., Revised effective ionic radii and systematic studies of interatomic distances in halides and chalcogenides. Acta Crystallographica Section A, 1976. 32(5): p. 751-767.
16. Saha, M., et al., Carrier concentration dependent optical and electrical properties of Ga doped ZnO hexagonal nanocrystals. Physical Chemistry Chemical Physics, 2015. 17(24): p. 16067-16079.
17. Abduev, A., et al., A revised growth model for transparent conducting Ga doped ZnO films: Improving crystallinity by means of buffer layers. Plasma Processes and Polymers, 2015. 12(8): p. 725-733.
18. Zhu, W., et al., Analysis of defect luminescence in Ga-doped ZnO nanoparticles. Physical Chemistry Chemical Physics, 2016. 18(14): p. 9586-9593.

19. Ajimsha, R.S., et al., Observation of weak localization and phase coherent electron transport in sparsely doped (Zn:Ga)O thin films. Journal of Alloys and Compounds, 2017. 708: p. 73-78.
20. Kim, J., et al., Optical Properties of Gallium-Doped Zinc Oxide\char22{}A Low-Loss Plasmonic Material: First-Principles Theory and Experiment. Physical Review X, 2013. 3(4): p. 041037.
21. Haifeng, Z., et al., Solvothermal synthesis of gallium-doped zinc oxide nanoparticles with tunable infrared absorption. Materials Research Express, 2014. 1(4): p. 045022.
22. Tian, Z.R., et al., Complex and oriented ZnO nanostructures. Nature Materials, 2003. 2(12): p. 821-826.
23. Djuriić, A.B., A.M.C. Ng, and X.Y. Chen, ZnO nanostructures for optoelectronics: Material properties and device applications. Progress in Quantum Electronics, 2010. 34(4): p. 191-259.
24. Bahramian, R., H. Eshghi, and A. Moshaii, Influence of annealing temperature on morphological, optical and UV detection properties of ZnO nanowires grown by chemical bath deposition. Materials and Design, 2016. 107: p. 269-276.
25. Zhang, C., et al., Large-area zinc oxide nanorod arrays templated by nanoimprint lithography: Control of morphologies and optical properties. Nanotechnology, 2016. 27(48).
26. Li, W., et al., Different morphologies of ZnO and their triethylamine sensing properties. Journal of Alloys and Compounds, 2017. 706: p. 461-469.
27. Cheng, H., et al., Influence of ZnO buffer layer on the electrical, optical and surface properties of Ga-doped ZnO films. Journal of Alloys and Compounds, 2017. 705: p. 598-601.
28. Nomoto, J., H. Makino, and T. Yamamoto, High-Hall-Mobility Al-Doped ZnO Films Having Textured Polycrystalline Structure with a Well-Defined (0001) Orientation. Nanoscale Research Letters, 2016. 11(1).
29. Wang, H., et al., Growth and characterization of high transmittance GZO films prepared by sol-gel method. Thin Solid Films, 2016. 615: p. 19-24.
30. Gawali, S.A., et al., Synthesis of zinc oxide nanorods from chemical bath deposition at different pH solutions and impact on their surface properties. Journal of Alloys and Compounds, 2017. 704: p. 788-794.
31. Kurudirek, S.V., K.C. Pradel, and C.J. Summers, Low-temperature hydrothermally grown 100 μm vertically well-aligned ultralong and ultradense ZnO nanorod arrays with improved PL property. Journal of Alloys and Compounds, 2017. 702: p. 700-709.
32. Ding, Y., X.Y. Kong, and Z.L. Wang, Doping and planar defects in the formation of single-crystal ZnO nanorings. Physical Review B - Condensed Matter and Materials Physics, 2004. 70(23): p. 1-7.
33. Lucas, M., Z.L. Wang, and E. Riedo, Growth direction and morphology of ZnO nanobelts revealed by combining in situ atomic force microscopy and polarized

Raman spectroscopy. Physical Review B - Condensed Matter and Materials Physics, 2010. 81(4).
34. Dimitrov, O., et al., Gas sensitive ZnO thin films with desired (002) or (100) orientation obtained by ultrasonic spray pyrolysis. Materials Chemistry and Physics, 2014. 148(3): p. 712-719.
35. Liu, H., et al., Effect of annealing on structural and optical properties of ZnO/Al_2O_3 superlattice structures grown by atomic layer deposition at 150 °C. Journal of Alloys and Compounds, 2017. 703: p. 225-231.
36. Verde, M., et al., Soft solution processing of ZnO nanoarrays by combining electrophoretic deposition and hydrothermal growth. Materials Chemistry and Physics, 2013. 140(1): p. 75-80.
37. Peiteado, M., et al., Multipod structures of ZnO hydrothermally grown in the presence of Zn3P2. Materials Research Bulletin, 2010. 45(11): p. 1586-1592.
38. Byrappa, K. and T. Adschiri, Hydrothermal technology for nanotechnology. Progress in Crystal Growth and Characterization of Materials, 2007. 53(2): p. 117-166.
39. Greene, L.E., et al., Low-temperature wafer-scale production of ZnO nanowire arrays. Angewandte Chemie - International Edition, 2003. 42(26): p. 3031-3034.
40. Yoshimura, M. and K. Byrappa, Hydrothermal processing of materials: Past, present and future. Journal of Materials Science, 2008. 43(7): p. 2085-2103.
41. Zhang, J., et al., Controllable hydrothermal synthesis of ZnO nanowires arrays on Al-doped ZnO seed layer and patterning of ZnO nanowires arrays via surface modification of substrate. Applied Surface Science, 2011. 257(23): p. 10134-10140.
42. Baghbanzadeh, M., et al., A critical assessment of the specific role of microwave irradiation in the synthesis of ZnO micro-and nanostructured materials. Chemistry - A European Journal, 2012. 18(18): p. 5724-5731.
43. Mahpeykar, S.M., J. Koohsorkhi, and H. Ghafoori-Fard, Ultra-fast microwave-assisted hydrothermal synthesis of long vertically aligned ZnO nanowires for dye-sensitized solar cell application. Nanotechnology, 2012. 23(16).
44. Pimentel, A., et al., Synthesis of long ZnO nanorods under microwave irradiation or conventional heating. Journal of Physical Chemistry C, 2014. 118(26): p. 14629-14639.
45. Phuruangrat, A., T. Thongtem, and S. Thongtem, Controlling morphologies and growth mechanism of hexagonal prisms with planar and pyramid tips of ZnO microflowers by microwave radiation. Ceramics International, 2014. 40(7 PART A): p. 9069-9076.
46. Ocakoglu, K., et al., Microwave-assisted hydrothermal synthesis and characterization of ZnO nanorods. Spectrochimica Acta - Part A: Molecular and Biomolecular Spectroscopy, 2015. 148: p. 362-368.
47. Bilecka, I. and M. Niederberger, Microwave chemistry for inorganic nanomaterials synthesis. Nanoscale, 2010. 2(8): p. 1358-1374.

48. Pan, L., et al., Nanophotocatalysts via microwave-assisted solution-phase synthesis for efficient photocatalysis. Journal of Materials Chemistry A, 2013. 1(29): p. 8299-8326.
49. Shi, W., S. Song, and H. Zhang, Hydrothermal synthetic strategies of inorganic semiconducting nanostructures. Chemical Society Reviews, 2013. 42(13): p. 5714-5743.
50. Bao, Y., C. Wang, and J.Z. Ma, Morphology control of ZnO microstructures by varying hexamethylenetetramine and trisodium citrate concentration and their photocatalytic activity. Materials and Design, 2016. 101: p. 7-15.
51. Talapin, D.V., et al., Prospects of colloidal nanocrystals for electronic and optoelectronic applications. Chemical Reviews, 2010. 110(1): p. 389-458.
52. Taubert, A., et al., Polymer-assisted control of particle morphology and particle size of zinc oxide precipitated from aqueous solution. Chemistry of Materials, 2002. 14(6): p. 2594-2601.
53. Calatayud, D.G., M. Rodríguez, and T. Jardiel, Controlling the morphology of TiO_2 nanocrystals with different capping agents. Boletín de la Sociedad Española de Cerámica y Vidrio, 2015. 54(4): p. 159-165.
54. Calatayud, D.G., et al., Highly photoactive anatase nanoparticles obtained using trifluoroacetic acid as an electron scavenger and morphological control agent. Journal of Materials Chemistry A, 2013. 1(45): p. 14358-14367.
55. Lin, H., et al., Size dependency of nanocrystalline TiO_2 on its optical property and photocatalytic reactivity exemplified by 2-chlorophenol. Applied Catalysis B: Environmental, 2006. 68(1-2): p. 1-11.
56. Look, D.C., et al., Self-compensation in semiconductors: The Zn vacancy in Ga-doped ZnO. Physical Review B - Condensed Matter and Materials Physics, 2011. 84(11).
57. Demchenko, D.O., et al., Impurity complexes and conductivity of Ga-doped ZnO. Physical Review B - Condensed Matter and Materials Physics, 2011. 84(7).
58. Zhang, Y., et al., Synthesis, characterization, and applications of ZnO nanowires. Journal of Nanomaterials, 2012. 2012.
59. Govender, K., et al., Understanding the factors that govern the deposition and morphology of thin films of ZnO from aqueous solution? Journal of Materials Chemistry, 2004. 14(16): p. 2575-2591.
60. Giraldi, T.R., et al., Effect of synthesis parameters on the structural characteristics and photocatalytic activity of ZnO. Materials Chemistry and Physics, 2012. 136(2-3): p. 505-511.
61. Distaso, M., et al., Influence of the counterion on the synthesis of ZnO mesocrystals under solvothermal conditions. Chemistry - A European Journal, 2011. 17(10): p. 2923-2930.
62. Guo, J., et al., Synthesis and conductive properties of Ga-doped ZnO nanosheets by the hydrothermal method. Materials Letters, 2013. 97: p. 34-36.

63. Bahadur, H., et al., Morphologies of sol-gel derived thin films of zno using different precursor materials and their nanostructures. Nanoscale Research Letters, 2007. 2(10): p. 469-475.
64. Padmanabhan, S.C., et al., Microwave-assisted synthesis of ZnO micro-javelins. Journal of Materials Chemistry, 2009. 19(48): p. 9250-9259.
65. Erwin, S.C., et al., Doping semiconductor nanocrystals. Nature, 2005. 436(7047): p. 91-94.
66. Bernardo, M.S., et al., Intrinsic compositional inhomogeneities in bulk Ti-doped $BiFeO_3$: Microstructure development and multiferroic properties. Chemistry of Materials, 2013. 25(9): p. 1533-1541.
67. Bernardo, M.S., et al., Sintering and microstuctural characterization of W^{6+}, Nb^{5+} and Ti^{4+} iron-substituted $BiFeO_3$. Journal of Alloys and Compounds, 2011. 509(26): p. 7290-7296.
68. Desu, S.B. and D.A. Payne, Interfacial Segregation in Perovskites .1. Theory. Journal of the American Ceramic Society, 1990. 73(11): p. 3391-3397.
69. Volanti, D.P., et al., Efficient microwave-assisted hydrothermal synthesis of CuO sea urchin-like architectures via a mesoscale self-assembly. CrystEngComm, 2010. 12(6): p. 1696-1699.